International Journal of Wavelets, Multiresolution
and Information Processing
Vol. 16, No. 1 (2018) 1850008 (17 pages)

DOI: 10.1142/S021969131850008X

World Scientific
www.worldscientific.com

A novel fast detection method of infrared LSS-Target in complex urban background

Yanfeng Wu*,†,‡, Haijiang Sun*,§ and Peixun Liu*,¶

*Fast Capture and Real-time Image Processing Technology Lab
Changchun Institute of Optics, Fine Mechanics and Physics
Chinese Academy of Sciences, Changchun 130033, P. R. China

†University of Chinese Academy of Sciences
Beijing 100049, P. R. China
‡wuyfciomp@yahoo.com
§sunhaijiang@126.com
¶liupeixun@126.com

Received 8 August 2017
Revised 19 October 2017
Accepted 20 October 2017
Published 21 November 2017

LSS-Target (the Low altitude, Slow speed and Small Target) is likely to be a threat to the observation platform, thus infrared LSS-Target detection is an urgent task. LSS-Target is a challenging issue due to the low Signal-to-Noise Ratio (SNR) and sophisticated background. Motivated by the analysis of infrared imaging characteristics, this paper proposes a novel fusion method for IR LSS-Target detection with complex urban background, which is suitable for precise guidance and self defense. First, an adaptive threshold segmentation based on accumulative histogram and maximum likelihood estimation are utilized to eliminate the clutter and improve SNR of the initial image. Second, a template is set up to identify the seed points in the image. Third, a constrained four criteria region growth algorithm is performed to separate the entire regions. Finally, the confidence measure is constructed, which can eliminate false targets and the background edges. Experimental results show that the method in this paper can screen out the real LSS-Target in real time with high accuracy under sophisticated background.

Keywords: Adaptive threshold segmentation; region growth; small target detection.

AMS Subject Classification: 22E46, 53C35, 57S20

1. Introduction

LSS-Target (the Low altitude, Slow speed and Small Target) is an aircraft or a floating object at a flight height lower than 2000 m and a speed less than 200 km/h.

As representatives, small aircraft, UAVS and aviation models develop fast in recent years. LSS-Target detection is widely used in searching, tracking and surveillance systems, consequently it is very important and urgent to detect the LSS-Target effectively in real time.

Many algorithms related to LSS-Target detection have been put forward in recent years, which can be grossly classified into two groups: single frame detection and sequential frames detection. Single frame detection finds targets without inter-frame prediction and compensation, which is of great concern in defense system. Yu *et al.* designed a Gaussian kernel to suppress the random noise and performed the region growth to filter out the large regions.[15] Fan *et al.* used morphology operators and correlation filter to extract characteristic vectors of small target.[6] Besides, particle filter,[1] median filter,[2] matched filter,[12] wavelet transformation[13] and Partial Differential Equation (PDE)[4,5] are commonly used in single frame detection. These algorithms can remove noises and enhance the contrast of image. However, they are not applicable to the complex urban area.

Sequential frames detection requires prior information and is able to process images with more complex background. Visual Background Extractor (ViBe) described by Barnich and Droogenbroeck is able to detect the LSS-Target in a static scene. ViBe can be initialized with a single frame, which is free of pause for the subsequent detection.[3] Nie *et al.* proposed a method, which models background after analyzing the image properties and detects the moving dim targets by Multi-level Hypothesis Testing (MHT).[11] Zhang *et al.* proposed a method based on Three-Fame Difference, which can perform real-time detection but with high false alarm rate.[16] Guariglia analyzed the entropies of Shannon, Rnyi and Kolmogorov[8] as well as Weierstrass–Mandelbrot Function[9] and computed fractional derivative of the Riemann zeta function, which is applicable and effective in IR image processing.[7,10]

In order to detect LSS-targets under dynamic and homogeneous background in real time, a novel fusion detection method with high accuracy is proposed in this paper. First, adaptive threshold segmentation based on accumulative histogram and maximum likelihood estimate are used to eliminate the clutter and improve the Signal-to-Noise Ratio (SNR). Second, a template is set up to identify the seed point in the image. Third, a constrained four criteria region growth algorithm is performed to separate regions. Finally, a small round target filter is constructed, which can eliminate false target and the background edges. Experimental results show that the performance of our method is better than Visual Background Extractor and Three Frame Difference method.

This paper includes the following structure and main contents: the first part is an introduction of the current research status. In Sec. 2, we analyze the features of LSS-Target. In Sec. 3, a detailed description about our method is given. The experimental results are provided in Sec. 4. Finally, we summarize the paper in the last section.

2. Features of LSS-Target

Due to the effects of atmospheric thermal noise, long distance transmission and noise of detection devices, LSS-Target usually exhibits the following three characteristics:

- The target spans a few pixels in the image, and the shape is similar to the point target;
- The SNR of the image under the remote camera is not high, and the target is usually hidden in the background;
- There are complex background such as buildings, woods and white cloud, which is conducive to ineffective detection of target.

The difficulties of small target detection are as follows:

- The lack of prior information of the background;
- Low SNR of the image makes it not easy to distinguish the background, the targets and the noises;
- The target may disappear from the background intermittently, which is difficult to predict;
- The lack of shape and texture features.

The infrared characteristics of LSS-Target are mainly the radiation caused by aerodynamic heating. When the target is moving, the surface of the target is heated by friction with the air, and the temperature of the target surface T_s can be calculated as follows:

$$T_s = T_0(1 + 0.16M^2), \tag{2.1}$$

where T_0 is the atmospheric temperature, and M is the Mach number, which is corresponding to the target velocity.

The Plank blackbody radiation law reveals the law of the black body radiation energy in terms of wavelength and temperature, and its mathematical expressions are as follows:

$$W_B(\lambda, T) = \frac{c_1}{\lambda^5} \cdot \frac{1}{(e^{c_2/\lambda T} - 1)}, \tag{2.2}$$

$$I_B(\lambda, T) = \frac{c_1}{\pi\lambda^5} \cdot \frac{1}{(e^{c_2/\lambda T} - 1)} = \frac{W_B(\lambda, T)}{\pi}, \tag{2.3}$$

where $W_B(\lambda, T)$ is the blackbody spectral irradiance, λ is the wavelength, T is the thermodynamic temperature of the blackbody radiation, the first radiation constant $c_1 = 3.742 \times 10^6\,\mathrm{W} \cdot \mathrm{m}^{-2}$, the second radiation constant $c_2 = 1.4388 \times 10^{-2}\,\mathrm{W} \cdot K$, $I_B(\lambda, T)$ is the spectral emissivity of the blackbody, which is the intensity of radiation emitted per unit area, unit time, and unit wavelength.

Assuming that the ambient temperature is 10°C and the target flight velocity is $0 - 2.5\,\mathrm{Ma}$, the spectral spectrum can be calculated by the formula Eqs. (2.1)–(2.3) and the peak wavelength is 6–10 μm.The peak wavelength of sky background

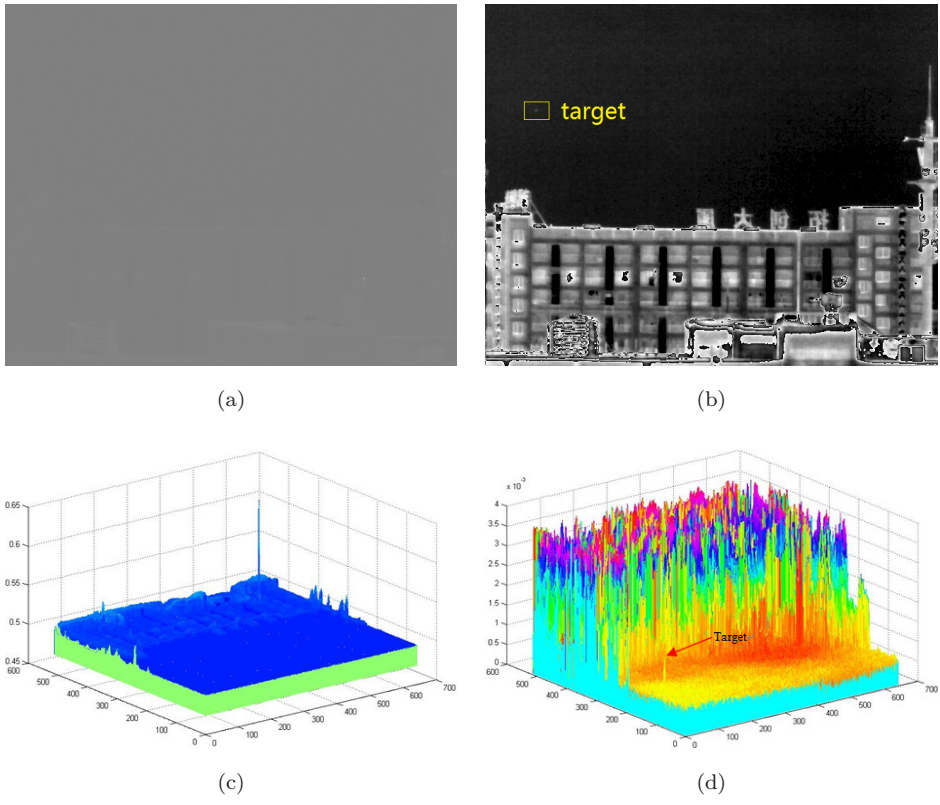

(a) (b)

(c) (d)

Fig. 1. Features of LSS-Target. (a) Original IR image. (b) Stretched image. (c) 3D-mesh view of the original image. (d) 3D-mesh view of the stretched image.

brightness during the day time is from 3 μm to 5 μm, and peak wavelength of sky background at night from 8 μm to 12 μm. So the temperature difference between background and target is relatively small, the gray value of the infrared image is low and concentrated. The energy distribution is shown in Fig. 1(a). A general IR image is modeled as Eq. (2.4)[14]

$$F(x, y) = T(x, y) + B(x, y) + N(x, y), \tag{2.4}$$

where $T(x, y)$ represents the target, $B(x, y)$ and $N(x, y)$ represent the background clutter and the noise, respectively.

The original image is a 16-bit gray scale image with a low contrast. It is quite impossible to find the target from the original image. In order to analyze the characteristic of the LSS-Target in the image, it is necessary to stretch 16-bit image into 8-bit image, and the formula is as follows:

$$s = T(r), \tag{2.5}$$

$$T(r) = \frac{255 \times (r - \min)}{(\max - \min)}, \tag{2.6}$$

where r is the gray value before transformation, and s is the gray value after transformation. Max is the maximum gray level in the image, and min is the minimum. The result is shown in Fig. 1(b).

From the results, it can be concluded that the gray values of the sky background and the urban area could be considered well-distributed, and the gray value of the urban area is larger than that of the sky background. What's more, the gray value of LSS-Target is between urban background and sky background.

3. Detection Algorithm

First of all, this paper uses double Gauss function to fit statistic histogram. Maximum likelihood estimation (MLE) is presented and used to calculate the threshold value and to extract the region of interest (ROI). Second, local maxima method is proposed to find pixels that belong to possible LSS-Target. Next, we perform the constrained four criteria region growth to filter out the large areas of clutter. Finally, we construct the confidence measure to screen out the real target from the candidate targets. Figure 2 is the flow chart of proposed method.

3.1. *The choice of ROI based on MLE and histogram statistic*

Under normal conditions, image with complex background always has different intensity distributions. Thus, to find the target, an effective and adaptive division method is needed.

The cumulative histogram represents the cumulative probability distribution of the image components at the gray level. Each value represents the probability of being less than or equal to the gray value. Consider the cumulative images histogram is a discrete function and the gray level is from 1 to $L-1$:

$$H(s_k) = n(k) \quad k = 0, 1, \ldots, L-1, \tag{3.1}$$

$$P(s_k) = \frac{H(s_k)}{n} \quad k = 0, 1, \ldots, L-1, \tag{3.2}$$

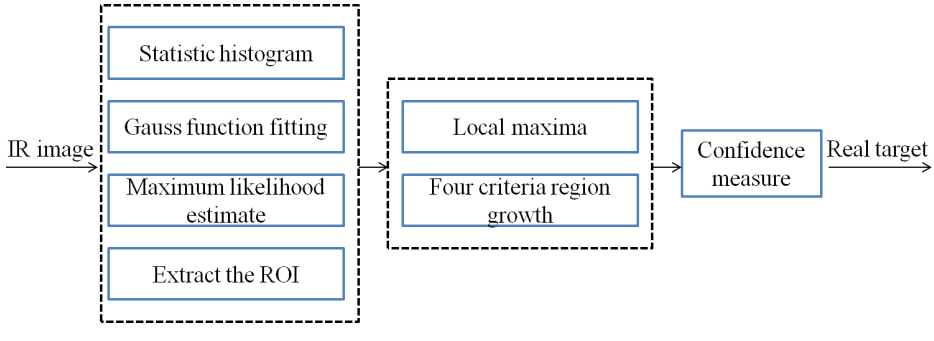

Fig. 2. Flow chart of proposed detection method.

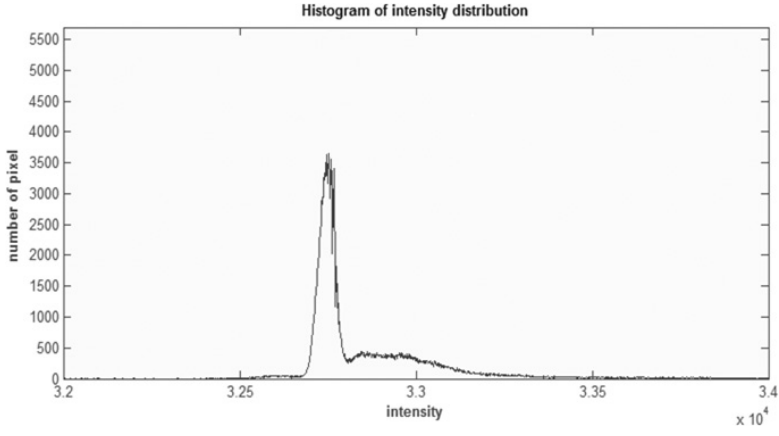

Fig. 3. Histogram of original IR image.

where n is the total pixels of the image and s_k is the value of gray level k. $n(k)$ is total pixels of s_k and $P(s_k)$ is the occurrence probability estimation of the gray level s_k.

Normally, for the images with many targets and a complex background has a multi-modal histogram. Histograms can be viewed as a superposition of multi-Gaussian distributions, for decomposition of multi-Gaussian can fit the multi-modal characteristics of histogram. The histogram of the original IR image is shown in Fig. 3. In this paper, double Gauss function is used to fit the histogram.

$$f(x) = a_1 \cdot \exp\left[-\left(\frac{x - b_1}{c_1}\right)^2\right] + a_2 \cdot \exp\left[-\left(\frac{x - b_2}{c_2}\right)^2\right], \tag{3.3}$$

where a_1, b_1, c_1, a_2, b_2 and c_2 are undetermined parameters. MLE is first proposed by C. F. Gauss in 1922, which can compute the probability density of the discrete random variables. In this paper, MLE is used to compute the unknown parameter of double Gauss function. Likelihood function L is as follows:

$$L(a_1, b_1, c_1, a_2, b_2, c_2) = \prod_{k=1}^{n} \left\{ a_1 \cdot \exp\left[-\left(\frac{n_k - b_1}{c_1}\right)^2\right] + a_2 \cdot \exp\left[-\left(\frac{n_k - b_2}{c_2}\right)^2\right] \right\}. \tag{3.4}$$

Taking logarithm

$$\ln L(a_1, b_1, c_1, a_2, b_2, c_2) = \sum_{k=1}^{n} \left\{ \ln a_1 \cdot \exp\left[-\left(\frac{n_k - b_1}{c_1}\right)^2\right] + a_2 \cdot \exp\left[-\left(\frac{n_k - b_2}{c_2}\right)^2\right] \right\}. \tag{3.5}$$

Solve the partial derivative of $\ln L$ with respect to a_1, b_1, c_1, a_2, b_2 and c_2, make them equal to zero, then we get

$$\begin{cases} \dfrac{\partial L(a_1,b_1,c_1,a_2,b_2,c_2)}{\partial a_1} \\ \quad = \displaystyle\sum_{k=1}^{n} \left\{ \frac{1}{a_1 + a_2 \cdot \exp\left[\left(\dfrac{n_k - b_1}{c_1} \right)^2 - \left(\dfrac{n_k - b_2}{c_2} \right)^2 \right]} \right\} = 0 \\ \dfrac{\partial L(a_1,b_1,c_1,a_2,b_2,c_2)}{\partial b_1} \\ \quad = \displaystyle\sum_{k=1}^{n} \left\{ \frac{\dfrac{2n_k}{{c_1}^2} - \dfrac{2b_1}{c_1}}{1 + \dfrac{a_2}{a_1} \cdot \exp\left[\left(\dfrac{n_k - b_1}{c_1} \right)^2 - \left(\dfrac{n_k - b_2}{c_2} \right)^2 \right]} \right\} = 0 \\ \dfrac{\partial L(a_1,b_1,c_1,a_2,b_2,c_2)}{\partial c_1} \\ \quad = \displaystyle\sum_{k=1}^{n} \left\langle \frac{2(n_k - b_2)^2}{{c_1}^3 \cdot \left\{ 1 + \dfrac{a_2}{a_1} \cdot \exp\left[\left(\dfrac{n_k - b_1}{c_1} \right)^2 - \left(\dfrac{n_k - b_2}{c_2} \right)^2 \right] \right\}} \right\rangle = 0 \end{cases} \tag{3.6}$$

$$\begin{cases} \dfrac{\partial L(a_1,b_1,c_1,a_2,b_2,c_2)}{\partial a_2} \\ \quad = \displaystyle\sum_{k=1}^{n} \left\{ \frac{1}{a_1 \cdot \exp\left[\left(\dfrac{n_k - b_2}{c_2} \right)^2 - \left(\dfrac{n_k - b_1}{c_1} \right)^2 \right] + a_2} \right\} = 0 \\ \dfrac{\partial L(a_1,b_1,c_1,a_2,b_2,c_2)}{\partial b_2} \\ \quad = \displaystyle\sum_{k=1}^{n} \left\{ \frac{\dfrac{2n_k}{{c_2}^2} - \dfrac{2b_2}{c_2}}{1 + \dfrac{a_1}{a_2} \cdot \exp\left[\left(\dfrac{n_k - b_2}{c_2} \right)^2 - \left(\dfrac{n_k - b_1}{c_1} \right)^2 \right]} \right\} = 0 \\ \dfrac{\partial L(a_1,b_1,c_1,a_2,b_2,c_2)}{\partial c_2} \\ \quad = \displaystyle\sum_{k=1}^{n} \left\langle \frac{2(n_k - b_1)^2}{{c_2}^3 \cdot \left\{ 1 + \dfrac{a_1}{a_2} \cdot \exp\left[\left(\dfrac{n_k - b_2}{c_2} \right)^2 - \left(\dfrac{n_k - b_1}{c_1} \right)^2 \right] \right\}} \right\rangle = 0, \end{cases} \tag{3.7}$$

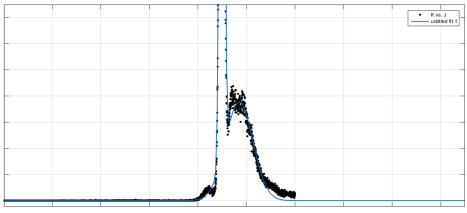

(a)

```
General model Gauss2:
     f(x) =  a1*exp(-((x-b1)/c1)^2) + a2*exp(-((x-b2)/c2)^2)
Coefficients (with 95% confidence bounds):
       a1 =        3376  (3369, 3382)
       b1 =   3.275e+04  (3.275e+04, 3.275e+04)
       c1 =       29.91  (29.84, 29.98)
       a2 =       376.8  (374.4, 379.1)
       b2 =   3.292e+04  (3.292e+04, 3.293e+04)
       c2 =       199.5  (197.8, 201.2)

Goodness of fit:
  SSE: 1.583e+07
  R-square: 0.9706
  Adjusted R-square: 0.9706
  RMSE: 15.54
```

(b)

Fig. 4. Fitting results. (a) Curve of double Gaussian fitting. (b) Result of parameters.

where a_1, b_1, c_1, a_2, b_2 and c_2 are the solutions of Eqs. (3.1), (3.6) and (3.7). The fitting results of Fig. 3 are shown in Fig. 4. According to Eq. (3.8), Q, the trough of the double Gaussian function as well as the threshold to extract the ROI of the image, can be obtained. Equation (3.9) is used to extract the ROI in the image.

$$\begin{cases} \left.\dfrac{\partial L(x)}{\partial x}\right|_{x=Q} = 0 \\ \lim\limits_{x \to Q^+} \dfrac{\partial L(x)}{\partial x} = 0 \\ \lim\limits_{x \to Q^-} \dfrac{\partial L(x)}{\partial x} = 0 \end{cases} \tag{3.8}$$

$$g(x,y) = \begin{cases} f(x,y), & g(x,y) < Q, \\ 0, & g(x,y) \geq Q, \end{cases} \tag{3.9}$$

where $f(x,y)$ is the gray value of the original image at (x,y), and $g(x,y)$ is the image after the preprocess.

3.2. *Marking the seed points*

The local energy of LSS-Target is aggregated, so the gray value of the pixel at the target always exhibits local maxima characteristics in the neighboring region. Thus, it is useful to perform a local maxima detection to mark seed points which may belong to a possible target. The local maxima detection can be performed by a $T \times T$ averaging template. The current point whose gray value is considerably higher than the average gray value of the neighbors in the template is marked as local maxima. Given a gray image f, the gray value of seed point $p(x,y)$ is $f(x,y)$, then the local maxima image of g is calculated as following:

3.3. *Constrained four criteria region growth*

Region growth is a normal step in target detection. Region growing is a method of combining pixels or sub regions into larger regions based on the predefined growth

Algorithm 1 Local Maxima Algorithm

Step 1: Setting $T \times T$ window to traverse the entire image, as shown in Fig. 5. The length of step is one.

Step 2: Calculate the mean of pixels in the $T \times T$ window with Eq. (3.10):

$$\text{median} = \frac{1}{T \times T} \sum_{i=-1}^{1} \sum_{j=-1}^{1} f(i,j). \tag{3.10}$$

.

Step 3: As shown in Eq. (3.11), comparing the difference between the mean values and the gray values of the pixels in the window. If the difference is beyond the threshold, then mark it as a seed point.

$$g(x,y) = \begin{cases} p(x,y), & \text{if } f(x,y) - \text{median} < \alpha, \\ 0, & \text{if } f(x,y) - \text{median} \geq \alpha, \end{cases} \tag{3.11}$$

where α is a threshold to evaluate how salient the LSS-Target is, compared to the background in the neighborhood, which is 10 in our case. The width of window T is 3 in our case. Some of the local maxima belong to small targets, but others may belong to the edges of background, which should be eliminated.

criteria. The basic processing method starts with a set of seed points to form the growth regions and the predefined attributed the neighborhood pixels are attached to each seed (such as the specified gray level or color). In order to get a suitable region growth result of the specific target detection, this paper proposed a constrained four criteria region growth method. The local maxima are considered to be the seeds to perform the region growth, and the region growth is performed according to the following steps:

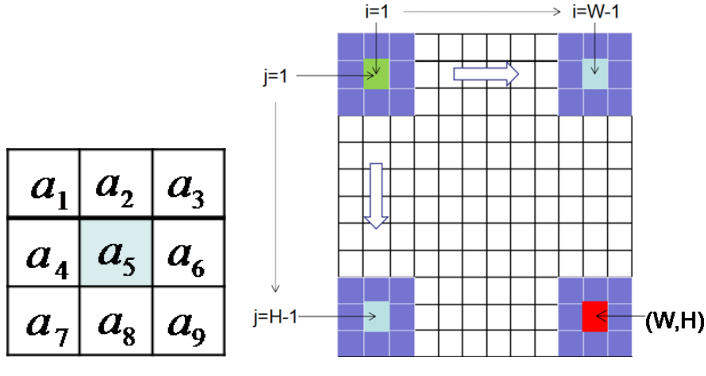

Fig. 5. (a) 3×3 template window. (b) The way of traversing the entire image.

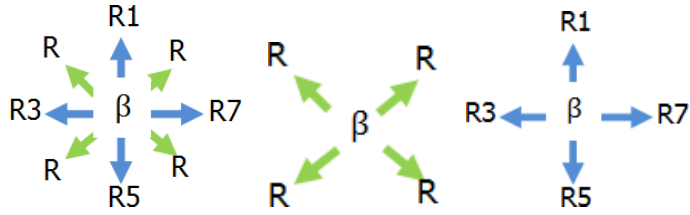

(a) (b) (c)

Fig. 6. Growth method. (a) Eight neighborhood. (b) Diagonal neighborhood. (c) Four neighborhood.

Algorithm 2 Four Criteria Region Growth Algorithm

Step 1: Traverse the entire image. When seed points are detected, set the eight neighborhood of the seed points as the region of interest. The gray value of the seed point is β and region of interest $R = \{R_1, R_2, R_3, R_4, R_5, R_6, R_7, R_8, R_9\}$, as shown in Fig. 6(a).
Step 2: Calculate the maximum of the gray value in the eight neighborhood with the seed point as the center ($R_{\max}$), $R_{\max} = \{R_1, R_2, R_3, R_4, R_5, R_6, R_7, R_8\}$.
Step 3: Search the four neighborhood (R_{n_1}) of the seed point in turn, $R_{n_1} = \{R_1, R_3, R_5, R_7\}$, as shown in Fig. 6(c). $P \in R_{n_1}$, if $p < R_{\max}$ and $|p - \beta| < \tau_1$, set P as the seed point. If $p = R_{\max}$ and $|p - \beta| < \tau_2$, set P as the seed point and update gray value (β) with the maximum value ($R_{\max}$).
Step 4: Search the seed point (R_{n_2}) in the eight domain except four points in the four neighborhood, as shown in Fig. 6(b), $R_{n_2} = \{R_2, R_4, R_6, R_8\}$. $P \in R_{n_2}$, if $p < R_{\max}$ and $|p - \beta| < \tau_3$, set P as the seed point. If $p = R_{\max}$ and $|p - \beta| < \tau_4$, set P as the seed point and update gray value (β) with the maximum value ($R_{\max}$).
Step 5: Repeat steps 2–4 until all of the seed points are processed, where $\tau_1 = 30, \tau_2 = 35, \tau_3 = 20, \tau_4 = 25$.

3.4. *Confidence measure of candidate targets*

For LSS-Target detection, it is expected to have a high detection rate and low false alarm rate. However, algorithm mentioned above can remove large areas of complex background clutter, there are still many edge areas and false targets that cannot be removed. In this paper, confidence measure is introduced to achieve the target detection.

Amplified LSS-Target is shown in Fig. 7, the area around the target is approximately the circular. The gray value of the target in the image increases first and decreases later, as shown in Fig. 8. Pixels change around the target and all sides have a gradient, as shown in Fig. 9.

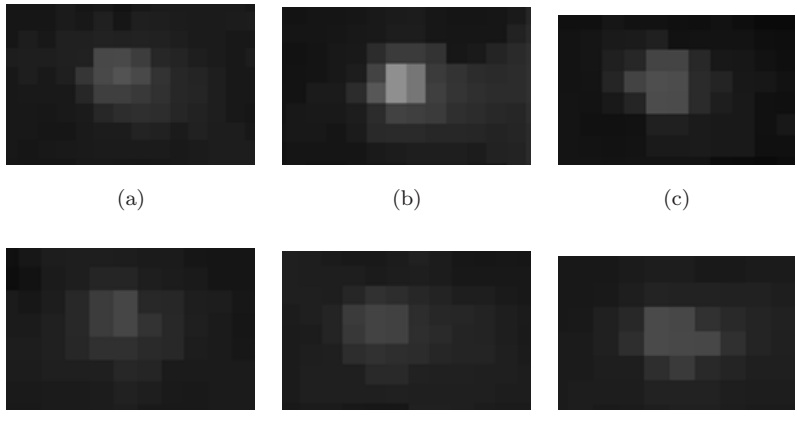

(a) (b) (c)

(d) (e) (f)

Fig. 7. Amplified target.

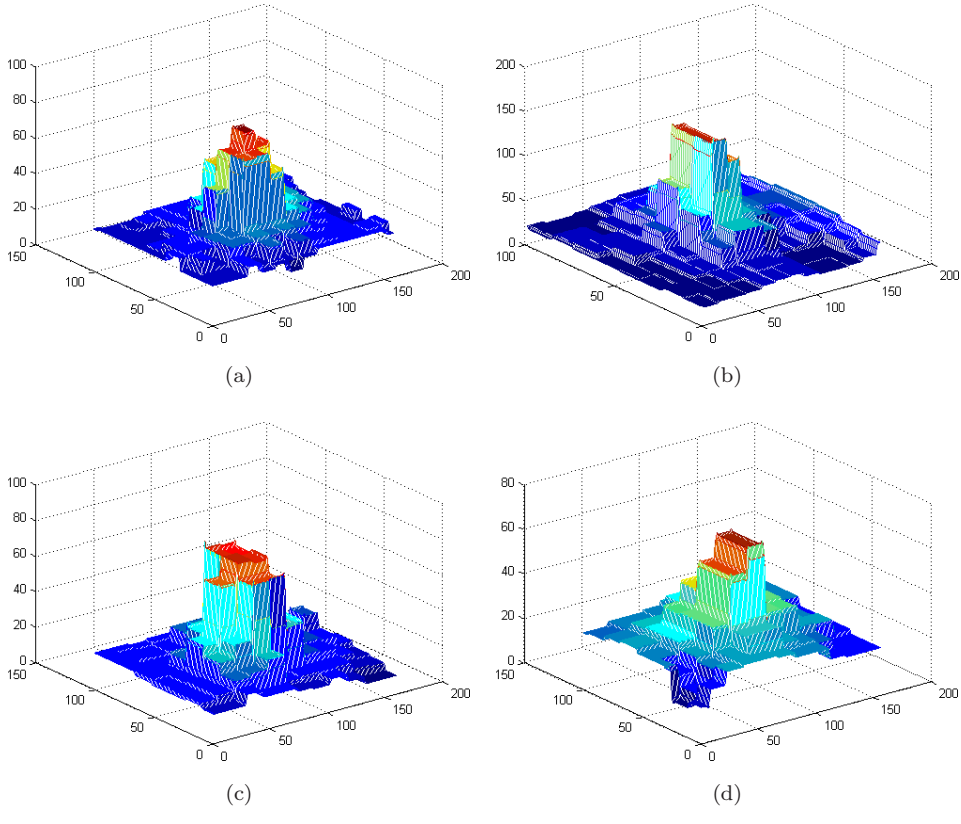

(a) (b)

(c) (d)

Fig. 8. 3D-mesh view of the amplified target.

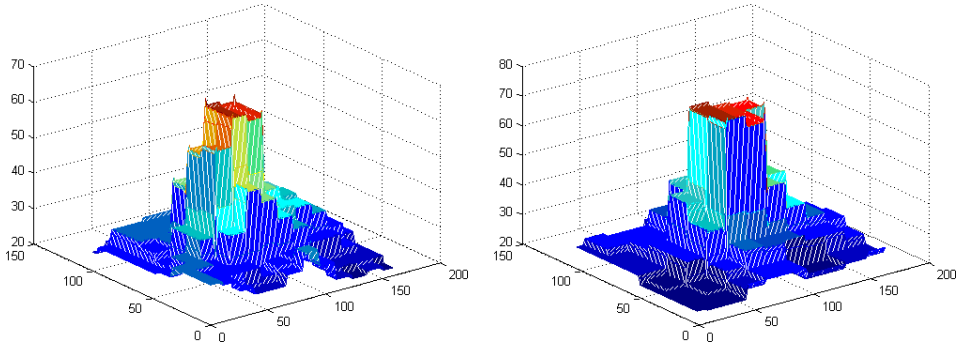

(e) (f)

Fig. 8. (*Continued*)

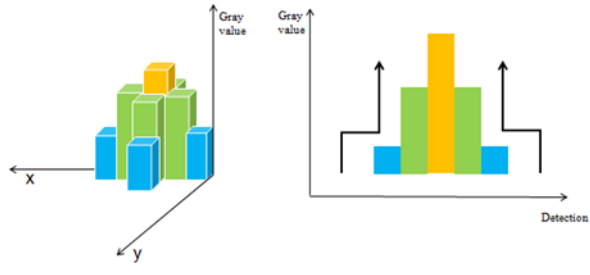

Fig. 9. Sketch map of gradient variety.

The confidence $C(A_i)$ takes the form

$$C(A_i) = C_1(A_i) \times C_2(A_i) \times C_3(A_i) \times C_4(A_i) \times C_5(A_i) \times C_6(A_i), \quad (3.12)$$

where C_1 shows the weight confidence

$$C_1(A_i) = \begin{cases} 0, & \text{if } w < \gamma_1, \\ 1, & \text{if } w \geq \gamma_1, \end{cases} \quad (3.13)$$

where w is the weight of candidate targets, C_2 shows the height confidence

$$C_2(A_i) = \begin{cases} 0, & \text{if } h < \gamma_2, \\ 1, & \text{if } h \geq \gamma_2, \end{cases} \quad (3.14)$$

where h is the height of candidate targets, C_3 shows the contour length confidence

$$C_3(A_i) = \begin{cases} 0, & \text{if } L < \gamma_3, \\ 1, & \text{if } L \geq \gamma_3, \end{cases} \quad (3.15)$$

where L is the contour length of candidate targets, C_4 shows the area confidence

$$C_4(A_i) = \begin{cases} 0, & \text{if } S < \gamma_4, \\ 1, & \text{if } S \geq \gamma_4, \end{cases} \quad (3.16)$$

where S is the area of candidate targets, C_5 shows the curvature confidence

$$C_5(A_i) = \frac{\mu_R}{\sigma_R}, \tag{3.17}$$

$$\mu_R = \frac{1}{k}\sum_{k=0}^{k-1} \|(x_k, y_k) - (\overline{x}, \overline{y})\|, \tag{3.18}$$

$$\sigma_R = \frac{1}{k}\sum_{k=0}^{k-1} [\|(x_k, y_k) - (\overline{x}, \overline{y})\| - \mu_R]^2, \tag{3.19}$$

$$\overline{x} = \frac{1}{S}\sum_{(x,y)\in R} x, \quad \overline{y} = \frac{1}{S}\sum_{(x,y)\in R} y, \quad S = \sum_{(x,y)\in R} 1, \tag{3.20}$$

where μ_R is the average distance from the center of the candidate region to the boundary of the candidate region. σ_R is the mean square deviation from the center of the candidate region to the boundary of the candidate region. Curvature confidence is monotonically increasing and approaches infinity, which is unaffected by regional translation, rotation and scale transformation where C_6 shows the intensity confidence

$$C_6(A_i) = \frac{1}{1 - e^{-\lambda_1(\mu_A - \mu_{A_i})}}, \tag{3.21}$$

where μ_A is the mean gray value of image, μ_{A_i} is the mean gray value of candidate target. The intensity confidence of LSS-Target is close to 1. $\gamma_1 = \gamma_2 = 5, \gamma_3 = 16, \gamma_4 = 3$ in this case.

4. Experimental Results and Analysis

In this experiment, we use an infrared camera to capture the .avi video file with LSS-Target and urban area. The whole image frames number is 1000 and the pixels of the frame is 640×512. The real target is 3 km away from the imaging system. The experiments were conducted on Microsoft Visual Studio 2010 software with a 3.2 GHZ Intel processor.

Fig. 10. The original 16-bit image.

Fig. 11. The results of adaptive threshold segmentation.

Fig. 12. The results of four criteria region growth.

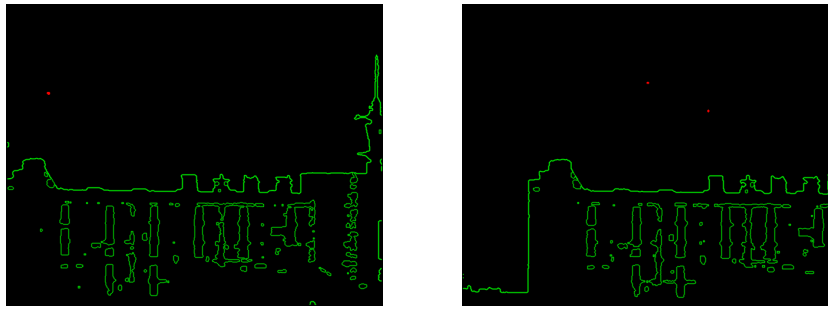

Fig. 13. Detection results. (Red points are the real target) (Color online).

The original image shown in Fig. 10. Figure 11 gives the detection results for the infrared image by using the histogram statistic and the maximum likelihood estimation. We can note that the fusion method can extract the target and the urban area clearly.

Figure 12 has presented the results of the local maxima and the constrained four criteria region growth. We can see from Fig. 12 that the large areas of urban background clutter are removed successfully.

Table 1. Statistical results of small target detection.

Algorithm	Total frames	Correct number	False alarm rate
This paper	100	93	14%
ViBe	100	61	46%
Three fame difference	100	46	7%

Table 2. The average time used by the small target detection.

Algorithm	Total frames	Second per frame (s)	Total time (s)
This paper	100	0.0857243	8.57243
ViBe	100	3.5663	35.663
Three fame difference	100	0.0366987	3.66987

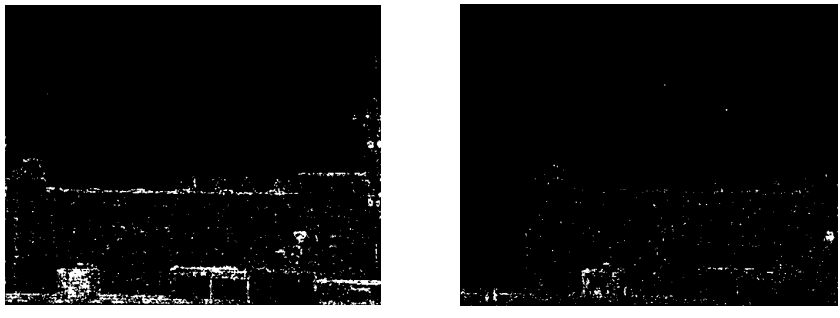

Fig. 14. The results of visual background extractor.

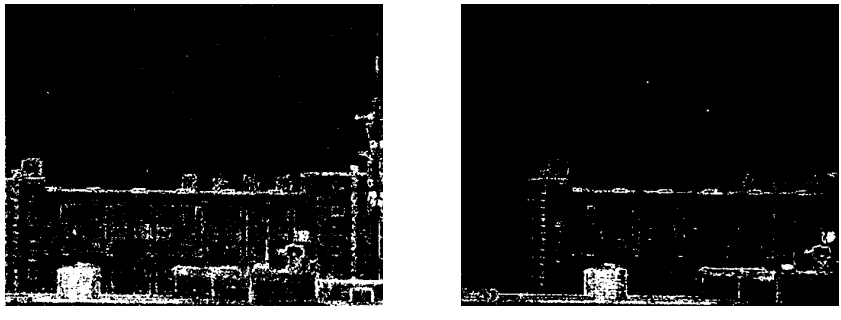

Fig. 15. The results of three fame difference.

Figure 13 shows the result of confidence measure, which can eliminate the false targets and detect the real target among candidate targets.

After observing the effect of algorithms proposed in this paper, we calculate the detection accuracy. Experiments demonstrate that the accuracy of the algorithm is up to 95.6%.

There are 64 frames in which the targets cannot be detected, for the difference of gray value between the target and the background are too small to segment. The average number of the false alarms per frame is 0.36.

To prove the advantages of the algorithm proposed in this paper, ViBe and three fame difference method is used to detect the same 100 frames. Time consumption is shown in Table 1, and the comparison is shown in Table 2. Figure 14 demonstrates the result of three fame difference method. Figure 15 shows the result of ViBe. Considering the time consumption and the detection accuracy, the algorithm proposed in this paper has the highest efficiency.

5. Conclusion

Based on the analysis of the feature of LSS-Target, we perform an impactful method in a complex background for LSS-target detection. At first, a novel algorithm based on the histogram statistic, the double-Gaussian fitting and the MLE are proposed to extract the ROI. Next, a template is created to detect the local maxima in the IR image, which is regarded as the seeds for the following region growth. A constrained four criteria region growth algorithm is performed to filter out the large areas of clutter. Finally, the confidence measure is proposed to screen out the real target from the candidate targets. This measure can filter out large regions, long regions and edges which cannot be targets. The experimental result shows that the proposed method significantly outperforms the existing methods in time-consuming and detection accuracy and can detect the moving infrared LSS-Target with complex urban background in real time.

References

1. B. Babenko, M. H. Yang and S. Belongie, Robust object tracking with online multiple instance learning, *IEEE Comput. Soc.* **33**(8) (2011) 1619–1632.
2. T.-W. Bae, Small target detection using bilateral filter and temporal cross product in infrared images, *Infrared Phys. Technol.* **54** (2011) 403–411.
3. O. Barnich and M. V. Droogenbroeck, VIBE: A powerful random technique to estimate the background in video sequences, *IEEE Trans. Image Process.* **20**(6) (2011) 1709–1927.
4. V. Caselles, R. Kimmel and G. Sapiro, Geodesic active contours, *Int. J. Comput. Vis.* **22**(1) (1997) 61–79.
5. T. F. Chan and L. A. Vese, Active contours without edges, *IEEE Trans. Image Process.* **10**(2) (2001) 266–277.
6. H. Fan, G. Ni and Y. Feng, A new algorithm for small and dim target detection of visible image under heavy clutters, *Opto-Electron. Eng.* **31**(6) (2004) 48–51.
7. E. Guariglia, C. Cattani and H. Srivastava, Fractional derivative of the Riemann zeta function, in Chap. 21, ed. X. J. Yang, *Fract. Dyn.* (2015), pp. 357–368.
8. E. Guariglia, Entropy and fractal antennas, *Entropy* **18**(03) (2016) 1–17.
9. E. Guariglia, Spectral analysis of the Weierstrass-Mandelbrot function, *2nd Int. Multidiscip. Conf. on Comput. Energy Sci.* (SpliTech), Split (2017), pp. 1–6.
10. E. Guariglia and S. Silvestrov, A functional equation for the Riemann zeta fractional derivative, *AIP Conf. Proc.* **1798** (2017), pp. 223–232.

11. H. Nie, Z. Huang, J. Diao, J. Chen, H. Liu and Q. Li, A wiener filter based infrared small target detecting and tracking method, *Intell. Syst. Design Eng. Appl.* **20**(1) (2010) 184–187.
12. I. S. Reed and R. M. Gagliardi, Optical moving target detection with 3-D matched filtering, *IEEE Trans. Aerospace Electron. Syst.* **24**(4) (1998) 327–336.
13. X. M. Shen and D. Li, Game theory approach to discrete H1filter design, *IEEE Trans. Signal Process.* **45**(4) (1997) 1092–1095.
14. Y. Wei, X. You and H. Deng, Small infrared target detection based on image patch ordering, *Int. J. Wavelets Multiresolut. Inf. Process.* **14**(02) (2016) 177–182.
15. H. Yu and B. Zhao, Detection of small targets of low SNR infrared images, *Laser Infrared* **34**(1) (2004) 40–42.
16. Y. Zhang, X. Wang and B. Qu, Three-frame difference algorithm research based on mathematical morphology, *Procedia Eng.* **29**(4) (2012) 2705–2709.